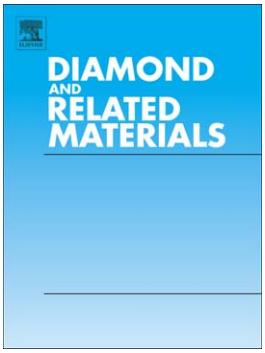

Improved surface coverage of an optical fibre with nanocrystalline diamond by the application of dip-coating seeding

Robert Bogdanowicz, Michał Sobaszek, Jacek Ryl, Marcin Gnyba, Mateusz Ficek, Łukasz Gołuński, Wojtek J. Bock, Mateusz Śmietana, Kazimierz Darowicki

PII: S0925-9635(15)00045-X
DOI: doi: 10.1016/j.diamond.2015.03.007
Reference: DIAMAT 6381

To appear in: *Diamond & Related Materials*

Received date: 2 November 2014
Revised date: 20 February 2015
Accepted date: 5 March 2015

Please cite this article as: Robert Bogdanowicz, Michał Sobaszek, Jacek Ryl, Marcin Gnyba, Mateusz Ficek, Łukasz Gołuński, Wojtek J. Bock, Mateusz Śmietana, Kazimierz Darowicki, Improved surface coverage of an optical fibre with nanocrystalline diamond by the application of dip-coating seeding, *Diamond & Related Materials* (2015), doi: 10.1016/j.diamond.2015.03.007

Improved surface coverage of an optical fibre with nanocrystalline diamond by the application of dip-coating seeding

Robert Bogdanowicz[1]*, Michał Sobaszek[1], Jacek Ryl[2], Marcin Gnyba[1], Mateusz Ficek[1], Łukasz Gołuński[1], Wojtek J. Bock[3], Mateusz Śmietana[4] and Kazimierz Darowicki[2]

[1] Department of Metrology and Optoelectronics, Faculty of Electronics, Telecommunications and Informatics, Gdansk University of Technology, 11/12 G. Narutowicza St., 80 233 Gdansk, Poland

[2] Department of Electrochemistry, Corrosion and Material Engineering, Faculty of Chemistry, Gdansk University of Technology, 11/12 Narutowicza St., 80 233 Gdansk, Poland

[3] Centre de recherche en photonique, Université du Québec en Outaouais, 101 rue Saint-Jean-Bosco, Gatineau, QC, J8X 3X7, Canada

[4] Institute of Microelectronics and Optoelectronics, Warsaw University of Technology, 75 Koszykowa St., 00-662 Warsaw, Poland

*****Author to whom correspondence should be addressed; e-mail: rbogdan@eti.pg.gda.pl; Tel.: +48-58-347-15-03; Fax: +48 58-347-18-48

Abstract: Growth processes of diamond thin films on the fused silica optical fibres (10 cm in length) were investigated at various temperatures. Fused silica pre-treatment by dip-coating in a dispersion consisting of detonation nanodiamond (DND) in dimethyl sulfoxide (DMSO) with polyvinyl alcohol (PVA) was applied. Nanocrystalline diamond (NCD) films were deposited on the fibres using the Microwave Plasma Assisted Chemical Vapour Deposition (MW PA CVD) method. The longitudinal variation of NCD morphology, structure and optical parameters were specifically investigated. The evolution of the film morphology and film thickness along the fibre length was studied using scanning electron microscopy (SEM). The chemical composition of the NCD film was examined with micro-Raman Spectroscopy. The sp^3/sp^2 band ratio was calculated using the Raman spectra deconvolution method. An approximately 5 cm-long homogeneous diamond film has been obtained on the surface of the fibre sample. Thickness, roughness and optical properties of NCD films in the VIS-NIR range were investigated on the reference quartz slides using spectroscopic ellipsometry. The samples exhibited relatively low deviations of refractive

index (2.3±0.25) and extinction coefficient (0.05±0.02) along the length of 5 cm, as estimated at a wavelength of 550 nm. In order to show the effectiveness of deposition process on optical fibres, diamond films were also grown on the fibre with induced long-period grating (LPG). The results of transmission measurements demonstrated that an LPG with diamond overlay exhibits the appropriate dependency on the optical properties of external medium. Thus, the deposition process has a negligible effect on the fibre transmission properties.

Keywords: Plasma CVD; Diamond film; Optical fibre coatings; Dip-coating seeding; Optical properties characterization; Long-period grating.

1. Introduction

Optical fibres have been extensively used for developing a number of sensing devices [1]. The advantages of fibre-based sensors include the resistance to high temperature, immunity to high electromagnetic field and electrical inertness. Various physical and chemical optical fibre sensors as well as devices capable of detecting gases [2,3], pH [4], temperature [5,6] or presence of biological molecules [6,7] have been developed. Optical fibres designed and fabricated mainly for the applications in telecommunication systems are typically covered with polymer coatings which protect the fibre against mechanical damages and harsh environmental conditions. However, the coating does not protect the fibre well against some acids.

Diamond films show a combination of properties which makes them attractive candidates for the application in sensing devices. These properties include, e.g., optical transparency in a broad wavelength range [8,9], chemical stability [10] and biocompatibility [7,11]. Moreover, the properties of diamond films can be easily tuned, i.e., *in situ* doping during the chemical vapour deposition (CVD) process effectively changes their electrical conductivity [12,13]. Diamond is also known for its high hardness. Diamond thin films can protect optical fibres against either mechanical damage or a chemically harsh environment. Thanks to their optical properties, which include a high refractive index and low optical absorption in the infrared spectral range, diamond thin films can also be applied for enhancing sensing properties of optical fibre devices [14].

Seeding is a key parameter influencing the diamond growth on various substrates [15–17]. This process can be performed via a number of methods [18], where the most commonly applied are ultrasonic treating of the substrate with the diamond slurry [19,20], coating the substrate with carbon-based materials [21], and the application of an interlayer that contains nanodiamond [22,23]. Poor

seeding results in a lack of continuity of the deposited films, the appearance of cracks, partial coverage of the substrates, large thickness gradient, or even a lack of film growth. Alberto *et al.* [24] reported the application of the Taguchi method as an efficient tool for targeting the appropriate conditions for fibre coating with nanocrystalline diamond. On the other hand, it is not trivial to achieve a good quality diamond-fibre interface due to a large difference in the properties and composition of the optical fibre material, i.e., fused silica, and diamond films [25]. May *et al.* [26] demonstrated that it is possible to deposit highly-resistive diamond films on optical fibres. Later, Rabeau *et al.* [27] produced nitrogen-doped diamond films deposited on the optical fibre end-face for fluorescence waveguiding. However, in the SEM images shown in [27] it can be seen that there is still room for improvement with regard to the homogeneity of diamond films produced. In our previous work we applied high-power sonication seeding in different suspensions (water / DMSO) for obtaining diamond films [28]. We have noticed that high power seeding can induce the erosion/cavitation of optical fibres. The application of titanium dioxide interlayer was also investigated; it was shown that a ~20 nm thick interlayer enhanced the growth of film on fused silica substrates [29].

Dip-coating seeding seems to be a promising method for the efficient seeding of optical fibres. This method does not employ any treatment that may damage the optical fibre. Moreover, it allows for easy treatment of long fibre sections. Scorsone *et al.* proposed seeding in a solution composed of polyvinyl alcohol (PVA) and detonation nanodiamond (DND) particles. PVA was chosen due to its ability to form thin films as well as its high viscosity and high solubility in water and surfactants [30,31].

To the best of our knowledge, neither the effect of dip-coating seeding in PVA/DMSO solution nor a study of spatial variation in morphology, structure and optical properties of diamond grown by chemical vapour deposition (CVD) on fused silica optical fibres has been reported yet. In the present study, we used PVA mixed with diamond slurry, the latter based on diethyl sulfoxide (DMSO) and diamond nanoparticles. The dispersion of particles in DMSO enables to achieve the higher concentration and low diameter of diamond particles (4-5 nm in size) [19,20]. Since optical fibres have a cylindrical shape we had to adopt a dip-coating method instead of typically used spin coating.

In this paper, we also discuss the spatial distribution of properties in nanocrystalline (NCD) diamond thin films deposited on long-period gratings that had been induced in fused silica. In our previous works, we investigated the properties of diamond films as determined at a single position only, and by using a different seeding pre-treatment [28,29]. Moreover, the measurements were performed on relatively short sections of optical fibres. High power sonication [28] enables to seed a short section of the fibre so it can only be used in tip sensing devices. Furthermore, the use of a TiO_2 interlayer [29] complicates the refractive index profile of LPG coverage, which additionally complicates the transmittance signal.

In the present work, we investigated several points on the substrate surface that correspond to the plasma distribution in the CVD chamber. Hu *et al.* [32,33] demonstrated that the optical properties of NCD films strongly depend on the deposition temperature. The substrate temperature has a crucial effect on the diamond film synthesis and the kinetics of pyrolytic reaction at the growth surface [34]. For this reason, the temperature dependence of plasma distribution and the homogeneity of diamond film growth on optical fibres have also been studied. In order to demonstrate the effectiveness of the deposition process on optical fibres, films were also grown on the fibre with induced long-period grating (LPG) for sensing purposes. The LPG is a periodic modulation of refractive index within the core of an optical fibre [35]. The modulation results in coupling of a core mode and a series of cladding modes. The coupling effect is observed as a series of resonances in the LPG transmission spectrum. Due to interactions between the modes, the resonance wavelengths depend on the fibre properties as well as the optical properties of external medium, which in this experiment is diamond overlay [36].

The NCD films were grown on fibres by microwave plasma assisted chemical vapour deposition (MW PA CVD). Scanning electron microscopy (SEM) imaging was applied to investigate the morphology of nanocrystalline diamond films. The chemical composition of the deposited layers was investigated by means of micro-Raman spectroscopy, while the deconvolution of Raman spectra was used to calculate the sp^3/sp^2 band ratio. The film growth rate, film thickness, and optical properties in the VIS-NIR range, i.e. refractive index and extinction coefficient were estimated on reference quartz slides by using spectroscopic ellipsometry (SE).

2. Experimental Section

2.1. Dip-coating system

In order to investigate the influence of dip-coating seeding on diamond growth, we prepared a single mode optical fibre (cleaved Corning SMF28, cladding diameter of 125 μm, approx. 10 cm in length) where the outer soft polyamide jacket was removed mechanically and the inner polyimide jacket was etched in the hydrogen plasma. The investigated optical fibre was composed of the fused silica cladding as an outer medium, which is high quality amorphous SiO_2, and of germanium-doped fused silica core as an inner medium (diameter of 8.2 μm). The quartz slides were used as reference samples for the deposition process on optical fibres. The fibres and quartz slides were cleaned for 5 minutes in an ultrasonic bath containing acetone, rinsed in 2-isopropanol and then dried.

Next, the optical fibres were subjected to hydrogenation. The process was performed in the microwave H_2 plasma at 1300W for 60 min. During the process the total flow of gas was reaching 300 sccm and the pressure was kept at a level of 50 Torr. Hydrogenation was supposed to remove

polyimide, which hinders the growth of diamond thin films. The seeding process included a double immersion of optical fibre in the suspension, each time for 1 min. In the second step, the fibre was turned around and its other end was dipped. The automatic dip-coating system was used for these purposes. Moreover, the reference quartz slides were seeded in the same seeding media by means of spin-coating. The suspension was prepared in a two-step procedure. Firstly, 1 g of solid PVA (average Molar Mass of 18000 g mol^{-1}) was suspended in 99 g of DMSO at a temperature of 80 $^{\circ}$C, resulting in a 1% w/w solution. Secondly, after the suspension had reached room temperature, 100 g of nanodiamond suspension (DMSO-DND 0.5% w/w) was carefully added.

2.2. Nanocrystalline diamond growth

Diamond films were synthesized using the MW PE CVD system (SEKI Technotron AX5400S, Japan). The optical fibres and reference quartz slides were placed in the CVD chamber on a molybdenum stage (see Figure 1).

Figure 1. Positioning of the samples in the CVD chamber during the diamond film growth. The fused silica optical fibres (2) and reference quartz slides (3) were placed on a Mo holder with a diameter of 10 cm (1).

The base pressure inside the chamber was 10^{-4} Torr. The chamber was filled with a mixture of hydrogen and methane. The chamber pressure was kept at 50 Torr with the total flow rate of gases reaching 300 sccm at the molar ratio of methane equal to 4 %. The plasma was generated with microwave radiation (2.45 GHz) and optimized for diamond synthesisat a power level of 1300 W [37–39].

Table 1. Description of samples and the corresponding deposition parameters. The letter X (assuming values from 1 to 5) codes various positions on the surface of the fibre sample as shown in Figure 1.

Sample	Substrate	Gas flow (sccm)	CH_4 (%)	T_c (^{o}C)	Time (min)
F300-SX	optical fibre	300	4	300	60
F475-SX	optical fibre	300	4	475	60
F550-SX	optical fibre	300	4	550	60
Q300-SX	quartz slide	300	4	300	60
Q475-SX	quartz slide	300	4	475	60
Q550-SX	quartz slide	300	4	550	60

The deposition time was kept at 60 min. The influence of the substrate temperature on fibre coating with diamond was specifically investigated. To this end, the molybdenum stage was heated by an induction heater and controlled by a thermocouple to reach T_c of 300, 475 or 550 °C during the process. Kromka *et al.* [40] reported that the low-temperature process (430 °C) results in a growth of well-faceted continuous films after the polymer-based seeding pre-treatment. The high-temperature process (830 °C) results in the formation of voids and openings in the deposited diamond layer. After reaching the desired temperature, the heating process was carried on for over 1 hour before starting plasma. The procedure was aimed at ensuring the equal temperature distribution across the Mo holder. After the growth process, the substrate temperature was slowly reduced (2 °C·min^{-1}) to room temperature. The temperature was adjusted by simultaneously lowering the microwave power and the current of induction heater. All the deposition parameters for each sample are listed in Table 1.

2.3. Analytical methods

The deposited diamond films were studied by advanced surface analysis techniques.

2.3.1. Scanning Electron Microscopy

The morphology studies were performed with a Hitachi S-3400N scanning electron microscope (SEM). A variable pressure SEM mode (VP-SEM) was used, which allows for assessing the sample morphology regardless of its electrical conductivity. A secondary electrons mode was applied with accelerating voltage reaching 20 kV. In order to quantify the variation of the cross-sectional non-uniformity, the NCD thickness was analyzed directly on the fibres by SEM. The NCD film thickness was estimated by using the graphical profiling in the program for data visualization and analysis (Gwyddion, 2.40, Czech Republic).

2.3.2. Raman Spectroscopy

The chemical composition of the deposited films was studied by means of Raman spectroscopy using Raman confocal microscope (Horiba LabRAM ARAMIS, Japan). Spectra were recorded in a range of 200–3500 cm^{-1} with an integration time of 5 s (10 averages), using a 532 nm diode pumped solid state (DPSS) laser in combination with a 50x objective magnification (*NA* = 0.5) and a 50 µm confocal aperture. The relative sp^3/sp^2 band ratios were determined by the deconvolution of Raman spectra using Gramms/AI Suite (Thermo Scientific, USA). Next, a comparison of the integral intensity of a band assigned to diamond (approx. 1332 cm^{-1}) and a wide "G" band assigned to the distorted sp^2 phase (between 1520 and 1600 cm^{-1}) was performed.

2.3.3. Spectroscopic Ellipsometry

SE analysis was carried out with a Jobin-Yvon UVISEL phase-modulated ellipsometer (HORIBA Jobin-Yvon Inc., Edison, USA) in a wavelength range from 260 to 830 nm. The experiments were performed at room temperature and with the angle of incidence fixed at 70º.

The ellipsometric fitting was based on a four-phase optical model (air/surface roughness film (SRL)/ diamond/ quartz). The dispersion of quartz was taken from the database [41]. The dielectric function of the SRL was estimated using the Bruggeman effective medium approximation (EMA). Diamond film was assumed to be an isotropic, homogeneous material and its dispersion was fitted to the Tauc-Lorentz oscillator (TL) model. This model has been recently used for amorphous semiconductors by Gioti *et al*. [42] and Logothetidis *et al.* [43]. Such materials exhibit a peculiarity due to the presence of two separated contributions of inter-band electronic transition related to the sp^2 and sp^3 bonded carbon [44]. The parameters of the TL model were fitted for each of the analyzed films.

Finally, the assumed optical model was fitted to the experimental data using the non-linear Levenberg-Marquardt regression method for mean-square error minimization (MSE) [45,46]. Based on the outcome of SE analysis, the thickness and optical constants, i.e. refractive index $n(\lambda)$ and extinction coefficient $k(\lambda)$ were obtained.

2.4. Long-period gratings (LPGs)

A set of LPGs was written with a computer-assisted precision arc-discharge apparatus, described in detail in [36]. The arc-induced LPGs show resistance to high temperatures, which is essential for the diamond growth process [47]. The arc-discharge system is based on a fusion splicer (Fitel, S182K, Japan) equipped with standard electrodes (Fitel, S182A, Japan), which are 2 mm wide and have a conical tip 4 mm in height. The constant tension of the fibre during the writing process was maintained with a 2 g weight. The grating period was set to Λ=403 μm, while the LPG length was 5 cm. The optical transmission of the fibre in a range of λ=1150-1650 nm was monitored during the LPG fabrication process in order to obtain the desired spectral attenuation notches.

In order to obtain the transmission measurements, we used a white light source (Yokogawa, AQ4305, Japan) and an optical spectrum analyser (Yokogawa, AQ6370B, Japan). The refractive index measurements for the LPG before and after the growth process were performed using several mixtures of glycerine and water with refractive indices (n_D) ranging from 1.33 to 1.47. The n_D value of the liquids was determined using an automatic refractometer (Rudolph Research Analytical, J57, USA) working with an accuracy of +/- $2 \cdot 10^{-5}$ refractive index unit (RIU).

3. Results and Discussion

3.1. Evolution of the surface morphology and chemical composition along the coated optical fibre

Figure 2 shows the SEM micrographs of the diamond layer morphology on the fibre and the quartz slide substrates for different deposition temperatures. The temperature of diamond growth has a strong influence on the plasma distribution and the pyrolysis of carbon precursor. The influence of temperature on the quality of diamond film has been demonstrated by Gicquel *et al.* [48]. The high crystallographic perfection of diamond films with different textures is obtained at moderate substrate temperatures (550 °C to 700 °C) in accordance with supersaturation (CH_3 density) and surface mobility (substrate temperature). For very low temperatures (<300 °C), spherical nano-particles are formed instead of the diamond phase.

In this study, the morphology of diamond films for the lowest temperature applied (300 °C) was similar to the diamond-like carbon or "cauliflower' structure, regardless of the substrate [49].

Figure 2. SEM micrographs of diamond films grown on the reference quartz slides (left) and fibres (right) at different substrate temperatures. Magnification is 10,000x.

In the case of the quartz slide substrates used in our experiment (samples Q475-S3 and Q550-S3), no difference in the grain size and homogeneity was detected. The values of mean grain diameter ranged from 100 to 300 nm. The homogeneous nanocrystalline structure of diamond film was achieved for sample F475-S3, with the mean grain size reaching half of that of quartz slide for the same substrate temperature. In the case of this particular sample, the diamond film was continuous and very homogeneous. On the other hand, at a higher temperature (550 °C) a lack of homogeneity and random crystallite size distribution was observed. Both these phenomena can be explained by worse adhesion of diamond to fused silica and spontaneous fracture behaviour in the quartz substrates, as was previously investigated by Kamiya *et al.* [50,51]. Furthermore, the cylindrical shape of a 125 µm in diameter fibre might have had a negative impact on homogeneity.

An increase in the crystallite size with increasing temperature has already been reported. Potocky *et al.* [52] investigated the influence of temperature on the growth of diamond film on the silicon and quartz substrates. The authors obtained homogeneous diamond films at temperatures below 400 °C; the films displayed a refractive index of 2.2.

In our study, the edges of crystallites are clearly visible and the film is uniform (Figure 3). A couple of centimetres closer to the edge of the holder (Figure 3 S4), the crystallites become smaller, while their shape is hard to define. At the edge of the holder (Figure 3 S5), a non-diamond coating is present. The amorphous diamond-like carbon structure with overgrown nanodiamond (ND) grain inclusions is noticeable in Figure 3 S5. It has to be pointed out that the observed ND possibly originated from the DND-PVA seeding suspension.

Figure 3. Longitudinal changes in morphology along F-475-SX fibre sample. The images were recorded 1 cm apart. Magnification is 10,000x.

Different processing techniques can be used for removing polyimide coating from the surface of fused silica optical fibre, i.e., thermal striping [53], chemical cleaning (boiling H_2SO_4 (aq) [54]; boiling 30% NaOH (aq) [55]) or laser removal [56]. In this work, a soft polyamide jacket was first mechanically removed. Next, the inner polyimide film was etched by the direct H_2-plasma treatment. The SEM micrographs showing the cross-sections of hydrogenated and non-hydrogenated fibres are presented in Figure 4AB. It is apparent that hydrogenation does not have any significant influence on the surface roughness.

In Figure 4A a diamond-coated fibre without the H_2 plasma pre-treatment is shown. In this case only the mechanical removal of soft outer polyamide jacket was performed. The delamination of diamond film is clearly visible.

Figure 4. SEM micrographs of the cross-sections of non-hydrogenated (A) and hydrogenated (B) NCD-coated fibres. The cross-sections of hydrogenated NCD-coated fibres in position S2 (D) and position S3 (E). Magnification is 1,000x. Insets: a SEM image showing the NCD coating (C) (magnification 20,000x) and the zoomed cross-sections characterized by marked non-uniformity at the measurement points (magnification 10,000x). The non-hydrogenated NCD-coated fibres were mechanically pre-treated to remove the soft outer polyamide jacket.

When fibre is covered with the protective polyimide film, it stands as an interlayer between the fibre and the diamond film. The delamination of diamond film from the coated sample can be explained by up to three orders of magnitude difference in the thermal expansion coefficient of fused silica (5.5×10^{-7} K^{-1}) [57] and polyimide film (1.1×10^{-4} K^{-1}) [58]. Furthermore, the temperature of the diamond film growth is higher than that of the molybdenum stage (300, 475 or 550 °C). It must be noted that there is no reliable method for measuring the temperature of the fibre substrates during the CVD process. Also, the pyrolysis of polyimide film may have partial impact on delamination. Dobrovol'skaya *et al.* [59], who investigated the thermal treatment of polyimide, concluded that the rate of pyrolytic reaction increases at temperatures above 490 ºC. The hydrogenated fibre coated with a homogeneous diamond thin film is shown in Figure 4B. Inset 4C presents a blow-up of the diamond-coated fibre in a cross-sectional view.

The employed hydrogen plasma processing of polyimide not only allows for the total removal of polymer, but it also enhances the seeding process. The exposure of the fibre surface to the hydrogen plasma results in changing the surface termination from Si-O to Si-OH. Such surface termination alters

the electrostatic nature of the fused silica surface, and strongly shifts zeta potential to negative values [15]. According to this scenario, the surface containing Si-OH groups undergoes protolysis and OH^- ions are adsorbed onto it [60]. Furthermore, this also indicates a change in wettability of the pre-treated surface. The measured average contact angle for a non-treated surface was 30° and that for the hydrogenated one was close to 0°. This fact allows for achieving a more uniform nucleation by means of spin-coating and for obtaining high nucleation densities [15]. The described process is a key issue in producing the smooth, uniform and continuous diamond films on the fused silica substrates.

In this study, DMSO-DND suspension was based on H-terminated nanodiamond. Williams *et al.* [61] showed that the hydrogen plasma treatment of nanodiamond results in a large shift of zeta potential from negative values up to +60 mV. The long-term stability of mixed PVA-DMSO-DND suspension suggests that a small admixture (0.5 % w/w) of PVA decreased only slightly the high positive values of zeta potential. Thus, the negative potential of the hydrogenated fused silica substrates attracts the positively-charged nanodiamond suspension, which results in the effective seeding density.

Due to the lack of other techniques suitable for the overlay thickness estimation directly on the cylindrical substrates, the authors applied SEM to assess the thickness of NCD deposited on the fibres The SEM analysis was carried out on the cross-sections of the cleaved parts of NCD coating. The authors present here the cross-sectional images of the middle part of the optical fibre (S2 in Fig. 4D) and the side part of S2 (S3 in Fig. 4E) taken from sample F-475-SX. Moreover, the insets (Fig.4; D1-E3) show the magnified regions at the boundary between the NCD film and the optical fibre.

In order to quantify the variation of the cross-sectional non-uniformity η_{CR} upon the point on the fibre (SX), we defined the non-uniformity of a microstructure as follows [62]:

$$\eta_{CR} = \frac{h_{edg} - h_{top}}{h_{top}} \cdot 100\% \qquad (1)$$

where h_{top} is the NCD thickness on the top side of a fibre (D1 or E1), and h_{edg} is the thickness in the middle or on the bottom side of an optical fibre (D2, D3 or E2, E3). The estimated values of thickness and non-uniformity factors of the NCD films deposited on the fibres have been summarized in Table 2.

Table 2. The values of thickness and non-uniformity factor of the NCD films deposited in the process coded F-475-SX as estimated by the analysis of SEM images.

Sample	Location (see Fig 4.)	Thickness (nm)	Cross-sectional uniformity (%)
F-475-S3	D1	240	-
F-475-S3	D2	212	-11.7
F-475-S3	D3	203	-15.4
F-475-S2	E1	221	-
F-475-S2	E2	217	-6.9

F-475-S2	E3	189	-16.3

A negative cross-sectional non-uniformity means that the thickness of the edge (D2/E2) or the bottom (D3/E3) side of the NCD coating is lower than the thickness at the point analysed on the top of the layer (D1/E1). The cross-sectional uniformity values were below 20 %. The obtained non-uniformities fell within the range of the roughness values estimated as SRL by spectroscopic ellipsometry (see Table 4). Furthermore, the NCD film thickness on the fibre (F-475) corresponded with the thickness values estimated on the reference fused silica substrates (Q-475) as summarized in Table 4. The highest thickness on the top of the fibre (D1/E1) was s controlled by the direct heating and the deposition from the plasma. The NCD growth at the bottom of the fibre required diffusion along the entire surface of the radial substrate.

The longitudinal non-uniformity of the NCD thickness was calculated by using a similar formula (1) and substituting h_{top} and h_{edg} with h_{E1} and h_{D1}, respectively. For the process coded F-475, the estimated longitudinal non-uniformity in position S3 compared to position S2 reached approx. -10%

It is apparent that the nature of the longitudinal or cross-sectional uniformity mostly originates from the temperature gradient. The variation of the substrate temperature is driven by two factors: (I) the disturbances in conduction heating via induction heat and (II) the density gradient of microwave power. The first factor that significantly influences the cross-sectional non-uniformity is the temperature gradient across the diameter of optical fibre. The second factor affects the longitudinal non-uniformity due to the ball-like plasma shape, and also has a partial effect on the cross-sectional non-uniformity due to the plasma sheath effect on the dielectric optical fibre substrate.

Moreover, the thickness non-uniformities could have originated from the altered gas chemistry due to oxygen-related species coming from the fused silica during the early growth stage. The oxygen admixture added to the hydrogen-methane plasma results in the increased film growth rates [63]. Thus, the spatial characterization of the plasma composition is required to understand the longitudinal differences in the NCD growth on fused silica.

Figure 5. Raman spectra of protective polyimide film on the fused silica fibre(a); the NCD film deposited at 475 ºC on the polyimide-covered optical fibre(b); and the NCD film deposited on the hydrogenated fibre (c).

The cross-sectional SEM images of the fibres do not show any changes in the cladding diameter (125 μm) and the fibre core diameter (~ 9 μm) due to temperature-induced stress and microwave power during the CVD process. This finding indicates that the process of CVD diamond film growth does not impair the waveguide structure of optical fibres.

For comparative purposes, the Raman spectra of diamond film deposited on the optical fibre coated with the protective polyimide film, and diamond film deposited on the H_2-plasma etched fused silica fibre are shown in Figure 5 (b) and (c), respectively. In Figure 5 (c), the Raman spectrum of soft polyimide jacket on the fibre is also presented to facilitate the comparative analysis. The presence of strong diamond bands at 1335 cm^{-1} (a layer on the polyimide-coated fibre) and at 1331 cm^{-1} (a layer on the plasma etched fibre) confirms that diamond can grow on both surface types. A slight difference in the Raman shift is caused by different stress forces at the film/substrate interface. Polyimide is built from smaller atoms bound by weaker bonds than those present in the fused silica. This results in the shift of diamond bands towards higher wavenumbers in the film deposited on polyimide, while in the film deposited on silica the shift is towards lower wavenumbers. Moreover, the Raman bands of NCD (1102 cm^{-1}) and polyacetylene (1471 cm^{-1}) can be observed in Figure 5 (b). In conclusion, it is necessary to strictly control the process of polyimide removal because polyimide film modifies the conditions of light propagation inside the optical fibre and diamond film.

A comparison of Raman spectra obtained for the NCD films deposited at different substrate temperatures is shown in Figure 6 (a). It is noticeable that the deposition conducted at 475 ºC allows for achieving the highest quality diamond film. However, a strong diamond band is also present at 1332 cm^{-1} for the substrate temperature of 550 ºC. This particular NCD film was not very homogeneous as confirmed by, e.g., the presence of an additional band at 1465 cm^{-1}, whose assignment is not obvious (it can be assigned to CH bending, polyacetylene, methylene, methyl, semi-circle breathing of aromatic rings, or amorphous carbon structures), and non-homogeneous spatial distribution of Raman spectra along the fibre (not shown here). These results are in good agreement with the outcome of SEM analysis. The spectrum obtained for the substrate temperature of 300 ºC shows that this particular film is the thinnest (an apparent band at 483-491 cm^{-1} assigned to fused silica), while the band intensity at 1332 cm^{-1} assigned to diamond is the weakest. For all NCD films grown on the quartz substrates, there was an evident peak at around 1133 cm^{-1} which is associated with trans-polyacetylene, as been previously reported by Ferrari et al. [64]. The trans-polyacetylene peak was slightly shifted towards 1130 cm−1 or 1140 cm^{-1} along the fibre length, probably due to the differences in the grain size of diamond.

Figure 6. Raman spectra of the NCD-coated fused silica fibres: (a) recorded in position S3 for different deposition temperatures, and (b) measured along the fibre length for the deposition temperature equal to 475 °C (F475-SX). The measurement position SX refers to Figure 1.

For the substrate temperature of 475 ºC, the changes in Raman spectra along the fibre length (Figure 6 (b)) showed that an approx. 4-5 cm long section of homogeneous diamond film was generated in the middle of the sample (between the positions S2 and S4). This homogeneity could also

be noticed in the spatial distribution of the main parameters of Raman spectra. The parameters describing the quality of diamond film are listed in Table 3. A strong Raman band between 1329 and 1334 cm^{-1} assigned to diamond, and the high value of the sp^3/sp^2 band ratio are noticeable. Due of the plasma temperature distribution along the fibre, the film quality decreased with approaching the end of the fibre (positions S1 and S5). This finding has been confirmed by a significant decrease in the band assigned to diamond and the low sp^3/sp^2 band ratio in this area of the fibre. The full width at half maximum (FWHM) of diamond band was in the range that is typical for the CVD diamond (9-10 cm^{-1}). The FWHM of diamond band only broadened (12 cm^{-1}) in position S1, where the sp^2/sp^3 ratio of the film decreased. The shifting of the Raman bands assigned to diamond and the changes of bandwidth (FWHM) are due to local stresses at the film/fibre interface, which results from non-epitaxial deposition of diamond on an amorphous substrate.

Table 3. The sp^3/sp^2 ratio of Raman bands, and the FWHM of the Raman band at 1332 cm^{-1} estimated along the fibre length. The measurement point SX refers to Figure 1.

Sample position	**sp^3/sp^2 (rel.)**	**FWHM (cm^{-1})**
Q475-S1	0.042	12
Q475-S2	0.182	9
Q475-S3	0.297	10
Q475-S4	0.208	10
Q475-S5	0.088	9

3.2. Optical properties of nanocrystalline diamond films

Due to the difficulty of taking ellipsometric measurements directly on the curved surface of optical fibres, the measurements were performed on the reference diamond films deposited on quartz slides during the same deposition process.

The applied fitting procedure resulted in the accurate values of film thickness, film roughness as well as dispersion of refractive index and extinction coefficient. The mean estimation error of *n* and *k* for the analysed samples was <5%. The longitudinal changes of the refractive index and extinction coefficient for the generated NCD films were estimated at 550 nm and later compared in Figure 7. We investigated the effect of the substrate temperature on the deposition process as well as the spatial distribution of film properties. The obtained values of refractive index were high, ranging from 2.1 to 2.4 for the NCD films deposited at 475 and 550 ºC. Hu *et al.* [32,33] reported the values of *n* between

2.31 and 2.34 for the NCD films, while Gupta *et al.* [65] determined the *n* values between 1.7 and 2.1 for the microcrystalline diamond (MCD) films at λ= 632 nm. The lower values of *n* (compared to single crystalline diamond) indicate the lower physical density of the films [49,66].

Figure 7. Variation of optical constants for the nanocrystalline diamond films obtained on quartz slides at various substrate temperatures. The measurement position SX refers to Figure 1.

The *k* values, which correspond to optical absorption in the deposited films, were below 0.1 at 550 nm, indicating low light absorption over the entire length of the optical fibre. Nevertheless, the samples deposited at 475 °C had higher *n* and lower *k* values compared to the samples obtained at 550 °C. Sample Q475 also exhibited lower deviation of optical constant in the central 5 cm-long section of the fibre (marked with dotted vertical lines in Figure 7). The length was optimized taking into consideration the application of NCD in the optical fibre grating devices [14].

Due to the relatively low variability of *n* along the analyzed fibre sample, the data related to the substrate temperature of 475 ºC have been selected for the spectral analysis. The variation of $n(\lambda)$ and $k(\lambda)$ for the NCD films deposited at 475ºC was estimated at various positions (S1-S5) along the fibre length (see Figure 8); the *n* value of single-crystal diamond (SCD) is also listed for comparative purposes. The actual content of the sp^3 and sp^2 phases and the grain-boundary disorder in the NCD film have a significant influence on how the estimates deviate from the reference value, i.e. *n* of SCD. All the deposited diamond films had normal dispersion. The optical constants decreased with increasing wavelength, exhibiting a typical behaviour near the band gap of electronic transition. Moreover, for all the NCD films, the optical constants did not shift in wavelength relative to each other.

Figure 8. Variability of *n* and *k* for diamond films grown at 475 °C. The reference values of *n* for SCD were plotted (♦) for comparative purposes [67].

The *n* and *k* values for the NCD films grown at the central holder positions (S2, S3 and S4) differ meaningfully from those obtained at the holder boundaries (S1 or S5). The films in the positions S2/S3/S4 displayed the higher *n* values (2.3-2.4) compared to the films deposited in the positions S1/S5, i.e. 4 cm away from the holder centre (2.1-2.25). It should be noted that the *k* values were similar for all the analyzed positions on the sample surface; *k* reached 0.15 at 300 nm and then decreased to 0.05 at 800 nm. The deposited NCD films exhibit high transparency for longer wavelengths (UV-NIR) [68]. The axial profiles of plasma composition have already been estimated numerically [69] and studied by emission spectroscopy [38,70] or molecular beam mass spectrometry

[71]. Those results were applied in our study during the optimization of experimental parameters for the CVD process.

Since *n* is correlated with the material's density [49,66], the results suggest that the density of the films deposited at 475 ºC is higher than that of the films grown at 300 or 550 ºC. It should be mentioned that the observed effects can be partially explained by the denser microcrystalline structure of NCD films deposited directly on quartz slides compared to that of the NCD films deposited directly on the fibres. The results obtained in our study correspond well with the SEM images shown in Figure 2, which has been discussed above.

The values of thickness and surface roughness (SRL) of the NCD films deposited at different temperatures are listed in Table 4. It is noteworthy that the deposition time was kept at 60 min for all the investigated samples. The dip-coating seeding results in the deposition of a uniform PVA-DMSO-DND nanolayer on the fibre therefore the procedure should not affect the thickness of the NCD film. Moreover, PVA evaporates during the initial stage of the CVD growth [30]. The most reasonable explanation for the observed variation in film thickness is that different kinetics of the plasma surface chemistry induces the NCD film non-uniformity [69,72–74]. It has been widely reported that the diamond growth kinetics is also influenced by the substrate temperature [52,72,75]. On the other hand, it is apparent that the mechanism of diamond growth is also driven by the substrate temperature. The NCD growth process is limited by the temperature-controlled pyrolysis reactions on the substrate surface. The most probable are disturbances in the hydrogen concentration, causing changes in the removal efficiency of the surface-bonded hydrogen [76]. The temperature gradient and radial changes in plasma densities would act to promote localized plasma reactions, such as those abovementioned increased/decreased atomic hydrogen concentrations near the growth surface [52]. Additionally, the change in the gas chemistry due to oxygen-related species coming from the fused silica during the early growth stage could also affect the process.

The SE results in Table 4 demonstrate that the temperature of 300 ºC is too low for depositing a uniform NCD film. It was observed that during deposition the plasma ball is confined in a very narrow area at the substrate holder, resulting in the effective film growth mostly in position S3. For the deposition temperatures of 475 and 550 ºC, we obtained very similar growth rates and roughness distributions at the analysed positions along the fibre length. The positions S1 and S5 (samples Q475 and Q550), characterized by the thinnest film, represent the plasma areas where methyl diamond precursors (CH_x) occur at lower densities. The efficient synthesis of diamond strongly depends on the formation of methyl group (CH_3^+) induced by plasma, which needs to overcome larger activation energy for the formation of diamond nuclei and, thereafter, requires the higher substrate temperature to enable the growth diamond films. Nevertheless, the carbon-to-fused silica interactions are inevitable,

which impedes the nucleation on the fused silica substrates [77]. This results in a very low growth rate and the deposition of amorphous non-diamond phases.

For the positions S2, S3 and S4, the film thickness of hundreds of nanometres was achieved (growth rate of 5 ± 1 nm min^{-1}). A comparable growth rate has already been reported for fused silica [52]. The deviation of the maximum film thickness reached ca. 20 %. The SRL values in this region were similar for all the samples, with the mean value of 24 ± 1 nm.

Table 4. The thickness and SRL of the deposited films as determined by spectroscopic ellipsometry at different positions on the fibre corresponding to those marked in Figure 1.

Sample position	**Q300**	**Q475**	**Q550**
	NCD film thickness (nm) / SRL thickness (nm)		
S1	48 / 8	69 / 45	57 / 17
S2	45 / 2	307 / 25	221 / 16
S3	112 / 11	273 / 23	230 / 28
S4	60 / 8	230 / 24	181 / 29
S5	55 / 4	75 / 50	83 / 12

The outcome of SE analysis confirmed the results obtained by means of SEM and Raman spectroscopy (see section 3.1), indicating a high refractive index and low absorption with small longitudinal deviation in the crucial range of the fibre length (S2-S4).

3.3. The effect of the NCD film deposition on an LPG

The transmission spectrum of the LPG before and after the NCD growth process is shown in Figure 9. The fibre transmission in the wavelength range between the resonances was unaffected by the deposition process. This result proves that a relatively long high-temperature deposition process had a negligible effect on the fibre properties, i.e., possible diffusion of germanium dopant out of the fibre core. However, the deposition process had a significant influence on the response of LPG, namely, it resulted in a decrease of the LPG resonance depth and the spectral shift for all the investigated external refractive indices. Two effects can be responsible for this scenario, i.e. high temperature during the deposition process, and the deposition of high-refractive-index diamond overlay. According to our previous work [78], electric-arc induced gratings are resistant to a high-temperature (<350 °C) process. However, in the case of the NCD growth, the temperature can be significantly elevated. It is known that the annealing temperature below 800 °C may induce the relaxation of residual axial stress frozen

in the fibre during the drawing process, which diminishes the grating period [35]. This results in a slight shift of resonances towards shorter wavelengths. A significant shift towards longer wavelengths may in turn be induced by the fibre elongation, which takes place at the annealing temperatures higher than 900 °C. In our experiment, the process temperature could induce the shift of resonance wavelength as well as lead to a decrease in the resonance depth [78]. The observed decrease in depth resulted from the lowered refractive index modulation at the LPG region due to high temperature.

In the present study, the deposition of high-refractive-index overlay had an important effect on the LPG transmission spectrum. An increase in the external refractive index, which has also been obtained as a result of the high-refractive index film deposition, induces a shift of resonances towards shorter wavelengths [78]. When certain conditions are fulfilled, i.e., the external refractive index is high enough (Figure 10 (a), for n=1.46309) or the high-refractive-index overlay is sufficiently thick [79], the resonances shift towards shorter wavelengths and finally take the spectral position of the resonances previously appearing at lower wavelengths. This effect can be clearly seen in Figure 10 (b), where for n_{ext}=1.44322, the resonance at λ=1630 nm increases its depth and shifts towards the position of the resonance initially appearing at λ=1570 nm. A similar effect has been observed for the LPG coated with a thin layer of high-refractive-index silicon nitride [78,79] or diamond-like carbon [14] thin films. In turn, the resonance at λ=1300 nm and a double resonance at 1390 and 1420 nm also shift towards shorter wavelengths with a tendency to assume the initial positions at 1220 and 1320 nm, respectively.

The effect of double resonance most probably resulted from the asymmetrical deposition of an overlay around the LPG, as it has also been observed for the asymmetrical LPGs [80]. In our previous studies with the application of the RF PECVD method for thin overlay deposition on LPGs, the resonances tended to significantly increase their depth with increasing refractive index [78,79]. In this work, the observed relatively shallow resonances probably resulted from a high-temperature deposition process, which is destructive to an LPG.

Moreover, the asymmetrical growth of NCD can be indirectly affected by the cylindrical shape of the substrate. The nucleation density and the nucleation rate, which influence the final variability of film thickness, are probably controlled by the presence of oxygen species originating from the reduction of SiO_2 in the fused silica substrate during deposition. Furthermore, it should be added that the NCD growth does not occur in the regions with seeding defects. A seeding defect could possibly appear at the contact point between the fibre and the Mo substrate holder. Thus, a certain part of the SiO_2 surface is always exposed to the plasma during the deposition process [81].

Figure 9. Comparison of the LPG transmission spectra before and after the deposition of diamond overlay for two selected external refractive indices (n_{ext}= 1.333 and 1.443 RIU).

Figure 10. A response of an LPG to the external refractive index n_{ext} in the sample (a) before and (b) after the deposition of diamond coating.

4. Conclusions

We have demonstrated that the conformal NCD films deposited on the fused silica fibres can be improved by the hydrogen plasma pre-treatment and seeding in a PVA-DMSO nanodiamond suspension with the dip-coating method. Moreover, the growth parameters of the proposed process have been optimized, resulting in a low-temperature growth of the NCD films on 10 cm-long sections of the optical fibres. The morphological analysis showed that up to 5 cm of the fibre length can be coated with the uniform nanocrystalline structure of the high sp^3 phase content. In order to quantify the variation of non-uniformity, the NCD thickness was assessed directly on the fibres by the analysis of SEM images. The cross-sectional measurements of non-uniformity resulted in the values below 20 %, while the longitudinal non-uniformity reached approx. 10% in the samples coated at 475 ^{o}C. The thickness non-uniformities could have originated from the altered gas chemistry due to oxygen-related species coming from the fused silica during the early growth stage.

Moreover, the analysis of Raman spectra demonstrated that the optimal conditions for diamond film deposition were achieved at the substrate temperature of 475 ºC. Due of the plasma temperature distribution along the fibre, the quality of NCD films decreased with approaching the end of the fibre (S1 and S5). A strong Raman band between 1329 and 1334 cm^{-1} assigned to diamond, and the high value of the sp^3/sp^2 band ratio were noticeable in all regions. The full width at half maximum (FWHM) of diamond band was in the range that is typical for the CVD diamond (9-10 cm^{-1}).

For a higher deposition temperature (550 ºC), less homogeneous films were obtained. This was probably caused by differing thermal expansion coefficients of polycrystalline diamond films and the amorphous fused silica substrate. In turn, the application of lower temperature (300 ºC) resulted in the significantly lowered growth rate of the film.

He high values of refractive index (range: 2.1-2.4) were achieved for the NCD films deposited at 475 and 550 ºC. The values of k obtained in this study were below 0.1 at λ=550 nm, indicating low absorption of the film over the whole length of the optical fibre.

The deviation of the maximum film thickness reached ca. 20%, with the mean surface roughness of 24 ± 1 nm. The most reasonable explanation for the observed distribution is that the thickness of NCD film is highly affected by different kinetics of the plasma surface chemistry at various distances from the holder centre. It was widely reported that the diamond growth kinetics is also influenced by the substrate temperature. Thus, the knowledge of spatial characterization of plasma composition and the temperature gradient is required to understand the longitudinal differences in the NCD growth on fused

silica. But obtaining such data is very complicated due to the nano-sized nature of the aforementioned process parameters and the condition of no interference with the diamond growth process.

Considering further studies, we propose that the substrate temperature of 475 ºC should be selected as the optimal temperature for depositing the NCD layers in optical devices, including the optical fibre gratings. The NCD film was also deposited on the fibre with a periodic refractive index modulated core. The results of transmission measurements demonstrated that the applied process has a negligible effect on the fibre transmission properties. However, the fibre structures, such as LPGs, may be affected by both high-temperature process and the NCD film deposition.

Acknowledgements

This work was supported by the Polish National Science Centre (NCN) under the Grant No. 2011/03/D/ST7/03541 and by the Polish National Centre for Research and Development (NCBiR) under the project No. LIDER/03/16/L-2/10. The DS funds of the Faculty of Electronics, Telecommunications and Informatics of the Gdansk University of Technology are also acknowledged.

References

[1] O.S. Wolfbeis, Fiber-Optic Chemical Sensors and Biosensors, Anal. Chem. 76 (2004) 3269–3284. doi:10.1021/ac040049d.

[2] H. Tai, T. Yoshino, H. Tanaka, Fiber-optic evanescent-wave methane-gas sensor using optical absorption for the 3.392-?m line of a He?Ne laser, Opt. Lett. 12 (1987) 437–439. doi:10.1364/OL.12.000437.

[3] G.Z. Xiao, A. Adnet, Z. Zhang, F.G. Sun, C.P. Grover, Monitoring changes in the refractive index of gases by means of a fiber optic Fabry-Perot interferometer sensor, Sens. Actuators Phys. 118 (2005) 177–182. doi:10.1016/j.sna.2004.08.029.

[4] S. Dong, M. Luo, G. Peng, W. Cheng, Broad range pH sensor based on sol–gel entrapped indicators on fibre optic, Sens. Actuators B Chem. 129 (2008) 94–98. doi:10.1016/j.snb.2007.07.078.

[5] E. Li, X. Wang, C. Zhang, Fiber-optic temperature sensor based on interference of selective higher-order modes, Appl. Phys. Lett. 89 (2006) 091119–091119–3. doi:10.1063/1.2344835.

[6] M. Jedrzejewska-Szczerska, R. Bogdanowicz, M. Gnyba, R. Hypszer, B.B. Kosmowski, Fiber-optic temperature sensor using low-coherence interferometry, Eur. Phys. J. Spec. Top. 154 (2008) 107–111. doi:10.1140/epjst/e2008-00526-1.

[7] M. Amaral, A.G. Dias, P.S. Gomes, M.A. Lopes, R.F. Silva, J.D. Santos, et al., Nanocrystalline diamond: In vitro biocompatibility assessment by MG63 and human bone marrow cells cultures, J. Biomed. Mater. Res. A. 87A (2008) 91–99. doi:10.1002/jbm.a.31742.

[8] J. Stotter, S. Haymond, J.K. Zak, Y. Show, Z. Cvackova, G.M. Swain, Optically Transparent Diamond Electrodes for UV-Vis and IR spectroelectrochemistry, Interface. 12 (2003) 33–38.

[9] X. Checoury, D. Néel, P. Boucaud, C. Gesset, H. Girard, S. Saada, et al., Nanocrystalline diamond photonics platform with high quality factor photonic crystal cavities, Appl. Phys. Lett. 101 (2012) 171115. doi:10.1063/1.4764548.

[10] M. Panizza, G. Cerisola, Application of diamond electrodes to electrochemical processes, Electrochimica Acta. 51 (2005) 191–199. doi:10.1016/j.electacta.2005.04.023.

[11] P. Bajaj, D. Akin, A. Gupta, D. Sherman, B. Shi, O. Auciello, et al., Ultrananocrystalline diamond film as an optimal cell interface for biomedical applications, Biomed. Microdevices. 9 (2007) 787–794. doi:10.1007/s10544-007-9090-2.
[12] W. Gajewski, P. Achatz, O.A. Williams, K. Haenen, E. Bustarret, M. Stutzmann, et al., Electronic and optical properties of boron-doped nanocrystalline diamond films, Phys. Rev. B. 79 (2009) 045206. doi:10.1103/PhysRevB.79.045206.
[13] R. Bogdanowicz, J. Czupryniak, M. Gnyba, J. Ryl, T. Ossowski, M. Sobaszek, et al., Amperometric sensing of chemical oxygen demand at glassy carbon and silicon electrodes modified with boron-doped diamond, Sens. Actuators B Chem. 189 (2013) 30–36. doi:10.1016/j.snb.2012.12.007.
[14] M. Smietana, J. Szmidt, M.L. Korwin-Pawlowski, W.J. Bock, J. Grabarczyk, Application of diamond-like carbon films in optical fibre sensors based on long-period gratings, Diam. Relat. Mater. 16 (2007) 1374–1377. doi:10.1016/j.diamond.2006.11.018.
[15] H.-J. Lee, H. Jeon, W.-S. Lee, Synergistic Interaction between Substrate and Seed Particles in Ultrathin Ultrananocrystalline Diamond Film Nucleation on SiO2 with Controlled Surface Termination, J. Phys. Chem. C. 116 (2012) 9180–9188. doi:10.1021/jp2117328.
[16] D.M. Gruen, Nanocrystalline Diamond Films1, Annu. Rev. Mater. Sci. 29 (1999) 211–259. doi:10.1146/annurev.matsci.29.1.211.
[17] Y. Lifshitz, C.H. Lee, Y. Wu, W.J. Zhang, I. Bello, S.T. Lee, Role of nucleation in nanodiamond film growth, Appl. Phys. Lett. 88 (2006) 243114–243114–3. doi:10.1063/1.2213019.
[18] Asmussen/Reinha, D.K. Reinhard, Diamond Films Handbook, CRC Press, 2002.
[19] O. Shenderova, S. Hens, G. McGuire, Seeding slurries based on detonation nanodiamond in DMSO, Diam. Relat. Mater. 19 (2010) 260–267. doi:10.1016/j.diamond.2009.10.008.
[20] O.A. Williams, O. Douhéret, M. Daenen, K. Haenen, E. Õsawa, M. Takahashi, Enhanced diamond nucleation on monodispersed nanocrystalline diamond, Chem. Phys. Lett. 445 (2007) 255–258. doi:10.1016/j.cplett.2007.07.091.
[21] A. Kromka, O. Babchenko, H. Kozak, K. Hruska, B. Rezek, M. Ledinsky, et al., Seeding of polymer substrates for nanocrystalline diamond film growth, Diam. Relat. Mater. 18 (2009) 734–739. doi:10.1016/j.diamond.2009.01.023.
[22] M. Tsigkourakos, T. Hantschel, S.D. Janssens, K. Haenen, W. Vandervorst, Spin-seeding approach for diamond growth on large area silicon-wafer substrates, Phys. Status Solidi A. 209 (2012) 1659–1663. doi:10.1002/pssa.201200137.
[23] E.I. Givargizov, V.V. Zhiraov, A.V. Kuznetsov, P.S. Plekhanov, Growth of diamond particles on sharpened silicon tips, Mater. Lett. 18 (1993) 61–63. doi:10.1016/0167-577X(93)90057-5.
[24] N.J. Alberto, R. Simões, R.N. Nogueira, V.F. Neto, Optimisation of tailored diamond coating conditions onto optical fibres through the Taguchi method, Diam. Relat. Mater. 43 (2014) 60–65. doi:10.1016/j.diamond.2014.01.014.
[25] M. Śmietana, M. Dudek, M. Koba, B. Michalak, Influence of diamond-like carbon overlay properties on refractive index sensitivity of nano-coated optical fibres, Phys. Status Solidi A. 210 (2013) 2100–2105. doi:10.1002/pssa.201300059.
[26] P.W. May, C.A. Rego, M.N.R. Ashfold, K.N. Rosser, G. Lu, T.D. Walsh, et al., CVD diamond-coated fibres, Diam. Relat. Mater. 4 (1995) 794–797. doi:10.1016/0925-9635(94)05279-4.
[27] J.R. Rabeau, S.T. Huntington, A.D. Greentree, S. Prawer, Diamond chemical-vapor deposition on optical fibers for fluorescence waveguiding, Appl. Phys. Lett. 86 (2005) 134104. doi:10.1063/1.1890484.
[28] R. Bogdanowicz, M. Śmietana, M. Gnyba, Ł. Gołunski, J. Ryl, M. Gardas, Optical and structural properties of polycrystalline CVD diamond films grown on fused silica optical fibres pre-treated by high-power sonication seeding, Appl. Phys. A. 10.1007/s00339-014-8355-x (2014). doi:10.1007/s00339-014-8355-x.
[29] R. Bogdanowicz, M. Śmietana, M. Gnyba, M. Ficek, V. Straňák, Ł. Goluński, et al., Nucleation and growth of CVD diamond on fused silica optical fibres with titanium dioxide interlayer, Phys. Status Solidi A. 210 (2013) 1991–1997. doi:10.1002/pssa.201300096.

[30] E. Scorsone, S. Saada, J.C. Arnault, P. Bergonzo, Enhanced control of diamond nanoparticle seeding using a polymer matrix, J. Appl. Phys. 106 (2009) 014908. doi:10.1063/1.3153118.
[31] R. Kiran, E. Scorsone, P. Mailley, P. Bergonzo, Quasi-Real Time Quantification of Uric Acid in Urine Using Boron Doped Diamond Microelectrode with in Situ Cleaning, Anal. Chem. 84 (2012) 10207–10213. doi:10.1021/ac301177z.
[32] Z.G. Hu, P. Hess, Optical constants and thermo-optic coefficients of nanocrystalline diamond films at 30–500 °C, Appl. Phys. Lett. 89 (2006) 081906–081906–3. doi:doi:10.1063/1.2243863.
[33] Z.G. Hu, P. Prunici, P. Hess, K.H. Chen, Optical properties of nanocrystalline diamond films from mid-infrared to ultraviolet using reflectometry and ellipsometry, J. Mater. Sci. Mater. Electron. 18 (2007) 37–41. doi:10.1007/s10854-007-9175-y.
[34] R.F. Davis, Diamond films and coatings development, properties, and applications, Noyes Pub., Park Ridge, N.J., 1993.
[35] G. Humbert, A. Malki, Electric-arc-induced gratings in non-hydrogenated fibres: fabrication and high-temperature characterizations, J. Opt. Pure Appl. Opt. 4 (2002) 194. doi:10.1088/1464-4258/4/2/313.
[36] W.J. Bock, J. Chen, P. Mikulic, T. Eftimov, A Novel Fiber-Optic Tapered Long-Period Grating Sensor for Pressure Monitoring, IEEE Trans. Instrum. Meas. 56 (2007) 1176–1180. doi:10.1109/TIM.2007.899904.
[37] R. Bogdanowicz, M. Gnyba, P. Wroczyński, Optoelectronic monitoring of plasma discharge optimized for thin diamond film synthesis, J. Phys. IV Proc. 137 (2006) 57–60. doi:10.1051/jp4:2006137011.
[38] R. Bogdanowicz, M. Gnyba, P. Wroczynski, B.B. Kosmowski, Optoelectronic system for monitoring of thin diamond layers growth, J. Optoelectron. Adv. Mater. 12 (2010) 1660–1665.
[39] R. Bogdanowicz, Investigation of H_2:CH_4 Plasma Composition by Means of Spatially Resolved Optical Spectroscopy, Acta Phys. Pol. A. 114 (2008) 33–38.
[40] A. Kromka, S. Potocky, B. Rezek, O. Babchenko, H. Kozak, M. Vanecek, et al., Role of polymers in CVD growth of nanocrystalline diamond films on foreign substrates, Phys. Status Solidi B. 246 (2009) 2654–2657. doi:10.1002/pssb.200982272.
[41] E.D. Palik, ed., Handbook of Optical Constants of Solids, Vol. 2, 1st ed., Academic Press, 1991.
[42] M. Gioti, D. Papadimitriou, S. Logothetidis, Optical properties and new vibrational modes in carbon films, Diam. Relat. Mater. 9 (2000) 741–745. doi:10.1016/S0925-9635(00)00244-2.
[43] M. Gioti, S. Logothetidis, Dielectric function, electronic properties and optical constants of amorphous carbon and carbon nitride films, Diam. Relat. Mater. 12 (2003) 957–962. doi:10.1016/S0925-9635(02)00222-4.
[44] G.E. Jellison, F.A. Modine, Parameterization of the optical functions of amorphous materials in the interband region, Appl. Phys. Lett. 69 (1996) 371–373. doi:doi:10.1063/1.118064.
[45] H. Tompkins, E.A. Irene, Handbook of Ellipsometry, William Andrew, 2005.
[46] R. Bogdanowicz, Characterization of Optical and Electrical Properties of Transparent Conductive Boron-Doped Diamond thin Films Grown on Fused Silica, Metrol. Meas. Syst. 21 (2014). doi:10.2478/mms-2014-0059.
[47] G. Rego, O. Okhotnikov, E. Dianov, V. Sulimov, High-temperature stability of long-period fiber gratings produced using an electric arc, J. Light. Technol. 19 (2001) 1574–1579. doi:10.1109/50.956145.
[48] A. Gicquel, K. Hassouni, F. Silva, J. Achard, CVD diamond films: from growth to applications, Curr. Appl. Phys. 1 (2001) 479–496. doi:10.1016/S1567-1739(01)00061-X.
[49] J. Robertson, Diamond-like amorphous carbon, Mater. Sci. Eng. R Rep. 37 (2002) 129–281. doi:10.1016/S0927-796X(02)00005-0.
[50] S. Kamiya, H. Takahashi, A. Kobayashi, M. Saka, H. Abé, Fracture strength of chemically vapor deposited diamond on the substrate and its relation to the crystalline structure, Diam. Relat. Mater. 9 (2000) 1110–1114. doi:10.1016/S0925-9635(99)00331-3.

[51] S. Kamiya, M. Sato, M. Saka, H. Abé, Fracture toughness estimation of thin chemical vapor deposition diamond films based on the spontaneous fracture behavior on quartz glass substrates, J. Appl. Phys. 82 (1997) 6056–6061. doi:10.1063/1.366473.
[52] S. Potocky, A. Kromka, J. Potmesil, Z. Remes, V. Vorlicek, M. Vanecek, et al., Investigation of nanocrystalline diamond films grown on silicon and glass at substrate temperature below 400 °C, Diam. Relat. Mater. 16 (2007) 744–747. doi:10.1016/j.diamond.2006.11.028.
[53] C.E. Barnes, R.A. Greenwell, G.W. Nelson, The Effect Of Fiber Coating On The Radiation Response Of Fluorosilicate Clad, Pure Silica Core Step Index Fibers, in: 1987: pp. 69–76. doi:10.1117/12.940685.
[54] A. Skontorp, Strength and failure mechanisms of polyimide-coated optical fibers, Proc.-SPIE Int. Soc. Opt. Eng. 3986 (2000) 240–251. doi:10.1117/12.388112.
[55] D. Kim, Y.R. Shen, Study of wet treatment of polyimide by sum-frequency vibrational spectroscopy, Appl. Phys. Lett. 74 (1999) 3314–3316. doi:10.1063/1.123329.
[56] J.R. Lankard Sr, G. Wolbold, Excimer laser ablation of polyimide in a manufacturing facility, Appl. Phys. A. 54 (1992) 355–359. doi:10.1007/BF00324201.
[57] A.D. Yablon, Optical Fiber Fusion Splicing, 2005 edition, Springer, Berlin ; New York, 2005.
[58] G. Elsner, J. Kempf, J.W. Bartha, H.H. Wagner, Anisotropy of thermal expansion of thin polyimide films, Thin Solid Films. 185 (1990) 189–197. doi:10.1016/0040-6090(90)90018-9.
[59] I.P. Dobrovol'skaya, M.K. Mokeev, Y.N. Sazanov, A.V. Gribanov, T.E. Sukhanova, Changes in the supramolecular structure of heat-resistant polyimide fibers in the course of thermal treatment, Russ. J. Appl. Chem. 79 (2006) 1178–1180. doi:10.1134/S1070427206070263.
[60] W. Schuetzner, E. Kenndler, Electrophoresis in synthetic organic polymer capillaries: variation of electroosmotic velocity and .zeta. potential with pH and solvent composition, Anal. Chem. 64 (1992) 1991–1995. doi:10.1021/ac00041a039.
[61] O.A. Williams, J. Hees, C. Dieker, W. Jäger, L. Kirste, C.E. Nebel, Size-Dependent Reactivity of Diamond Nanoparticles, ACS Nano. 4 (2010) 4824–4830. doi:10.1021/nn100748k.
[62] J.K. Luo, D.P. Chu, A.J. Flewitt, S.M. Spearing, N.A. Fleck, W.I. Milne, Uniformity Control of Ni Thin-Film Microstructures Deposited by Through-Mask Plating, J. Electrochem. Soc. 152 (2005) C36–C41. doi:10.1149/1.1833320.
[63] Yuasa, M., Low temperature diamond film fabrication using magneto-active plasma CVD, Diam. Relat. Mater. 1 (1992) 168–174. doi:10.1016/0925-9635(92)90019-K.
[64] A.C. Ferrari, J. Robertson, Origin of the $1150-{\mathrm{cm}}^{-1}$ Raman mode in nanocrystalline diamond, Phys. Rev. B. 63 (2001) 121405. doi:10.1103/PhysRevB.63.121405.
[65] S. Gupta, B.R. Weiner, G. Morell, Ex situ spectroscopic ellipsometry investigation of the layered structure of polycrystalline diamond thin films grown by electron cyclotron resonance-assisted chemical vapor deposition, J. Appl. Phys. 90 (2001) 1280–1285. doi:doi:10.1063/1.1384487.
[66] G. Davies, Properties and growth of diamond, INSPEC, the Institution of Electrical Engineers, 1994.
[67] E.D. Palik, Handbook of Optical Constants of Solids, Academic Press, 1998.
[68] A. Kromka, B. Rezek, Z. Remes, M. Michalka, M. Ledinsky, J. Zemek, et al., Formation of Continuous Nanocrystalline Diamond Layers on Glass and Silicon at Low Temperatures, Chem. Vap. Depos. 14 (2008) 181–186. doi:10.1002/cvde.200706662.
[69] K. Hassouni, A. Gicquel, M. Capitelli, J. Loureiro, Chemical kinetics and energy transfer in moderate pressure H2 plasmas used in diamond MPACVD processes, Plasma Sources Sci. Technol. 8 (1999) 494. doi:10.1088/0963-0252/8/3/320.
[70] M. Gnyba, R. Bogdanowicz, Design and simulation of excitation laser system for in-situ Raman monitoring, Eur. Phys. J. Spec. Top. 144 (2007) 209–214. doi:10.1140/epjst/e2007-00129-4.
[71] J. Petherbridge, P.W. May, S.R.J. Pearce, K.N. Rosser, M.N.R. Ashfold, Molecular beam mass spectrometry investigations of low temperature diamond growth using CO2/CH4 plasmas, Diam. Relat. Mater. 10 (2001) 393–398. doi:10.1016/S0925-9635(00)00593-8.
[72] A. Gicquel, K. Hassouni, F. Silva, J. Achard, CVD diamond films: from growth to applications, Curr. Appl. Phys. 1 (2001) 479–496. doi:10.1016/S1567-1739(01)00061-X.

[73] K. Hassouni, O. Leroy, S. Farhat, A. Gicquel, Modeling of H2 and H2/CH4 Moderate-Pressure Microwave Plasma Used for Diamond Deposition, Plasma Chem. Plasma Process. 18 (1998) 325–362. doi:10.1023/A:1021845402202.
[74] P.W. May, M.N.R. Ashfold, Y.A. Mankelevich, Microcrystalline, nanocrystalline, and ultrananocrystalline diamond chemical vapor deposition: Experiment and modeling of the factors controlling growth rate, nucleation, and crystal size, J. Appl. Phys. 101 (2007) 053115. doi:10.1063/1.2696363.
[75] A. Netto, M. Frenklach, Kinetic Monte Carlo simulations of CVD diamond growth—Interlay among growth, etching, and migration, Diam. Relat. Mater. 14 (2005) 1630–1646. doi:10.1016/j.diamond.2005.05.009.
[76] J. Stiegler, T. Lang, Y. von Kaenel, J. Michler, E. Blank, Activation energy for diamond growth from the carbon–hydrogen gas system at low substrate temperatures, Appl. Phys. Lett. 70 (1997) 173–175. doi:10.1063/1.118348.
[77] P.T. Joseph, T. Nyan-Hwa, C. Yi-Chun, C. Hsiu-Fung, L. I-Nan, Transparent ultrananocrystalline diamond films on quartz substrate, Diam. Relat. Mater. 17 (2008) 476–480. doi:10.1016/j.diamond.2007.10.013.
[78] M. Smietana, W.J. Bock, P. Mikulic, Effect of high-temperature plasma-deposited nano-overlays on the properties of long-period gratings written with UV and electric arc in non-hydrogenated fibers, Meas. Sci. Technol. 24 (2013) 094016. doi:10.1088/0957-0233/24/9/094016.
[79] M. Smietana, W.J. Bock, P. Mikulic, Temperature sensitivity of silicon nitride nanocoated long-period gratings working in various surrounding media, Meas. Sci. Technol. 22 (2011) 115203. doi:10.1088/0957-0233/22/11/115203.
[80] X. Liu, M. Yan, L. Zhan, S. Luo, Z. Zhang, Y. Xia, Controlling of symmetric and asymmetric mode coupling in long-period fiber gratings singe-side induced by long-pulse CO2 laser, Opt. Commun. 284 (2011) 1232–1237. doi:10.1016/j.optcom.2010.11.027.
[81] S.A. Catledge, Y.K. Vohra, P.B. Mirkarimi, Low temperature growth of nanostructured diamond on quartz spheres, J. Phys. Appl. Phys. 38 (2005) 1410. doi:10.1088/0022-3727/38/9/013.

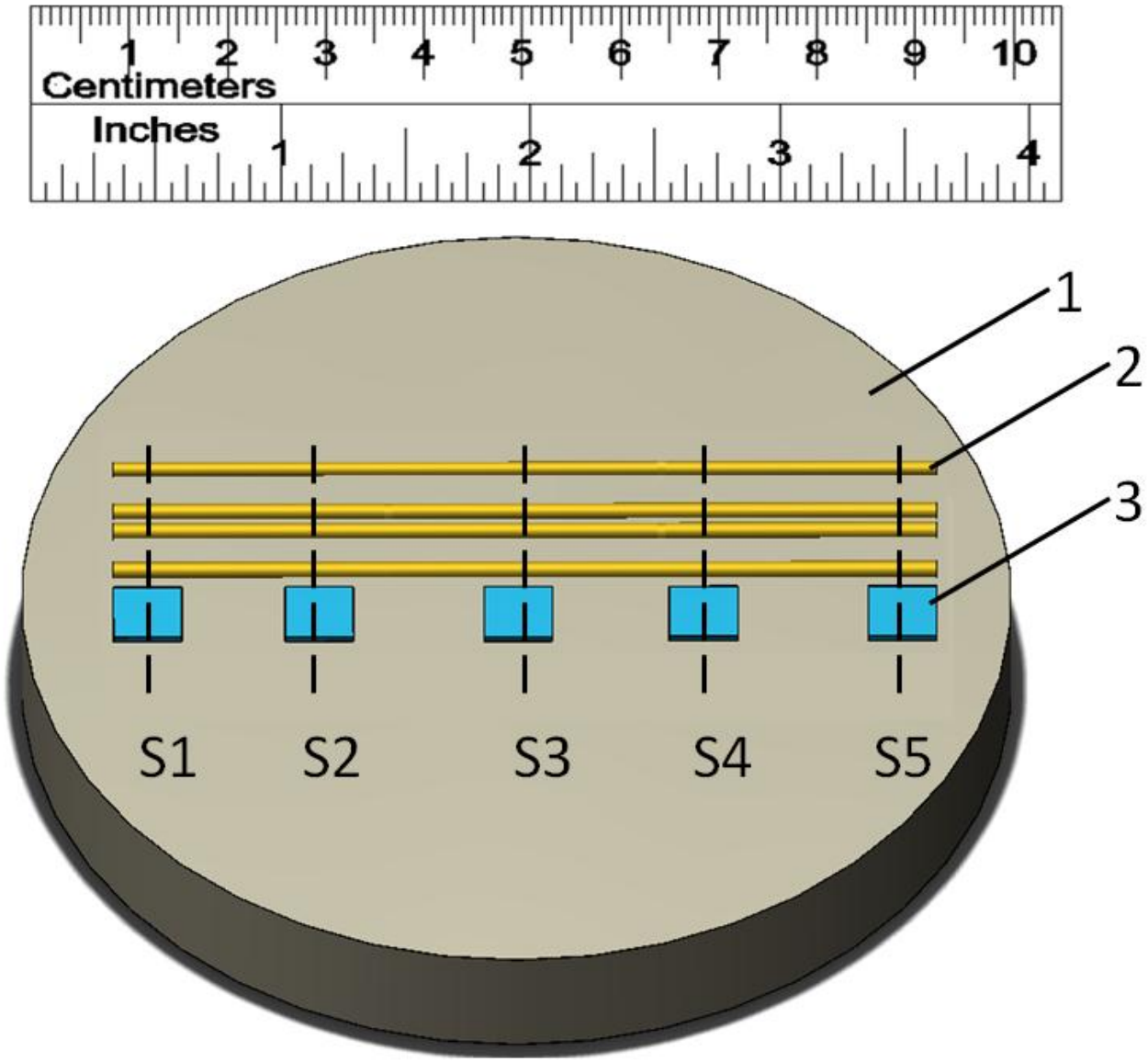

Fig. 1

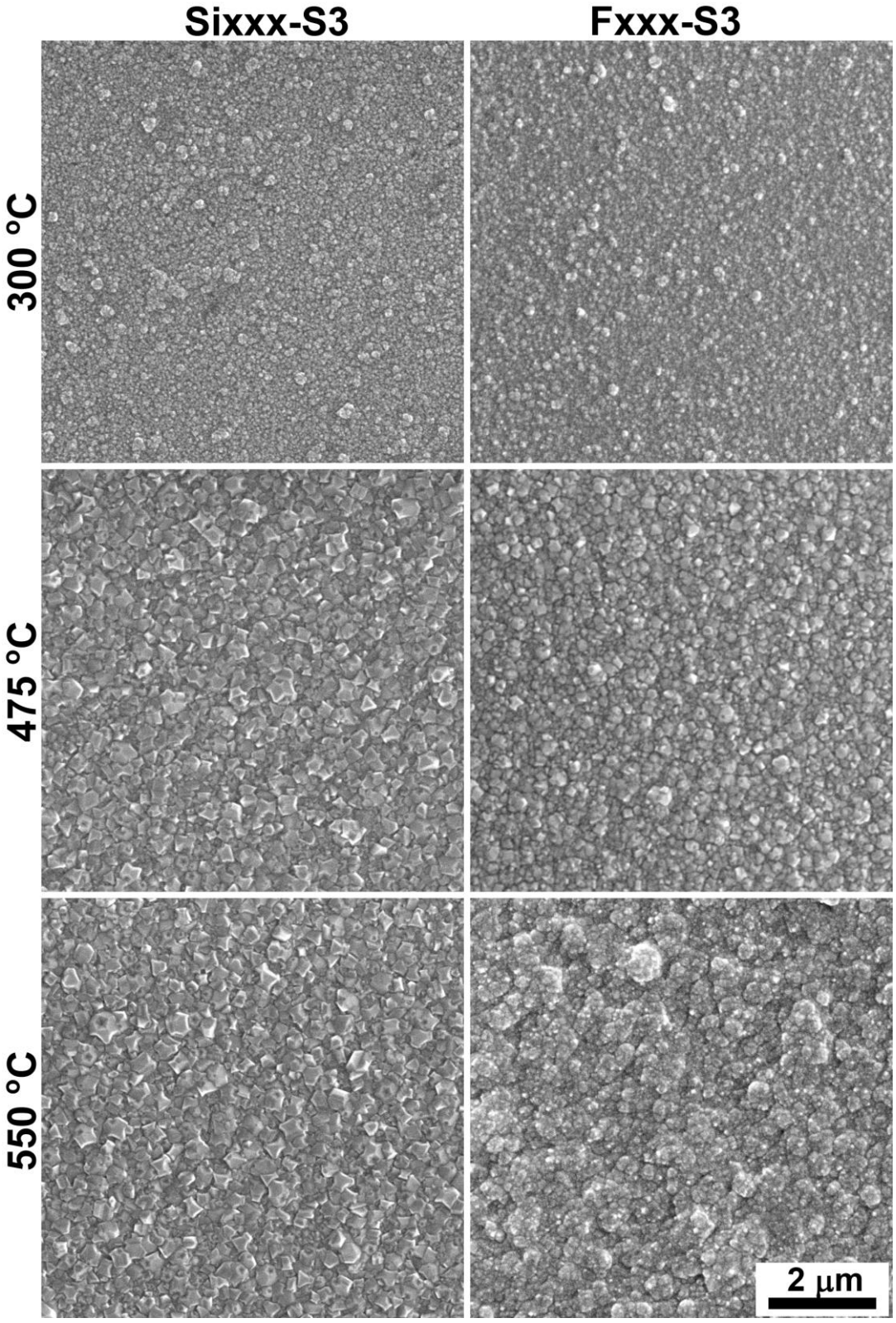

Fig. 2

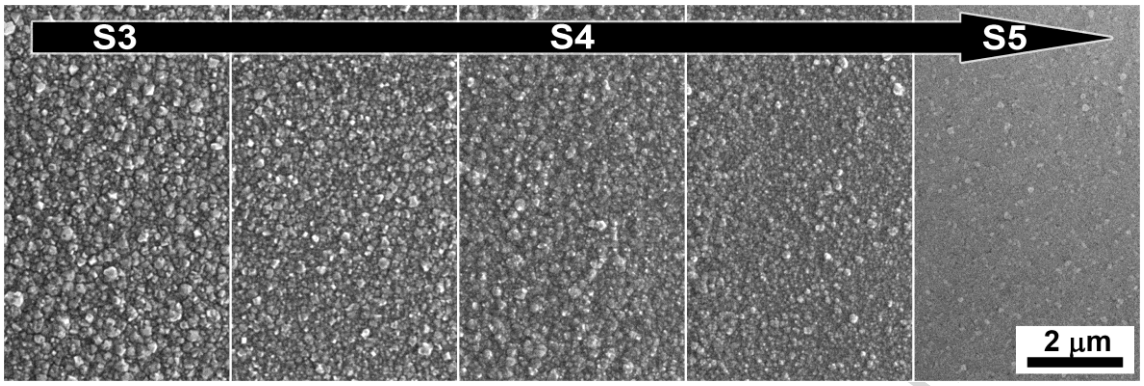

Fig. 3

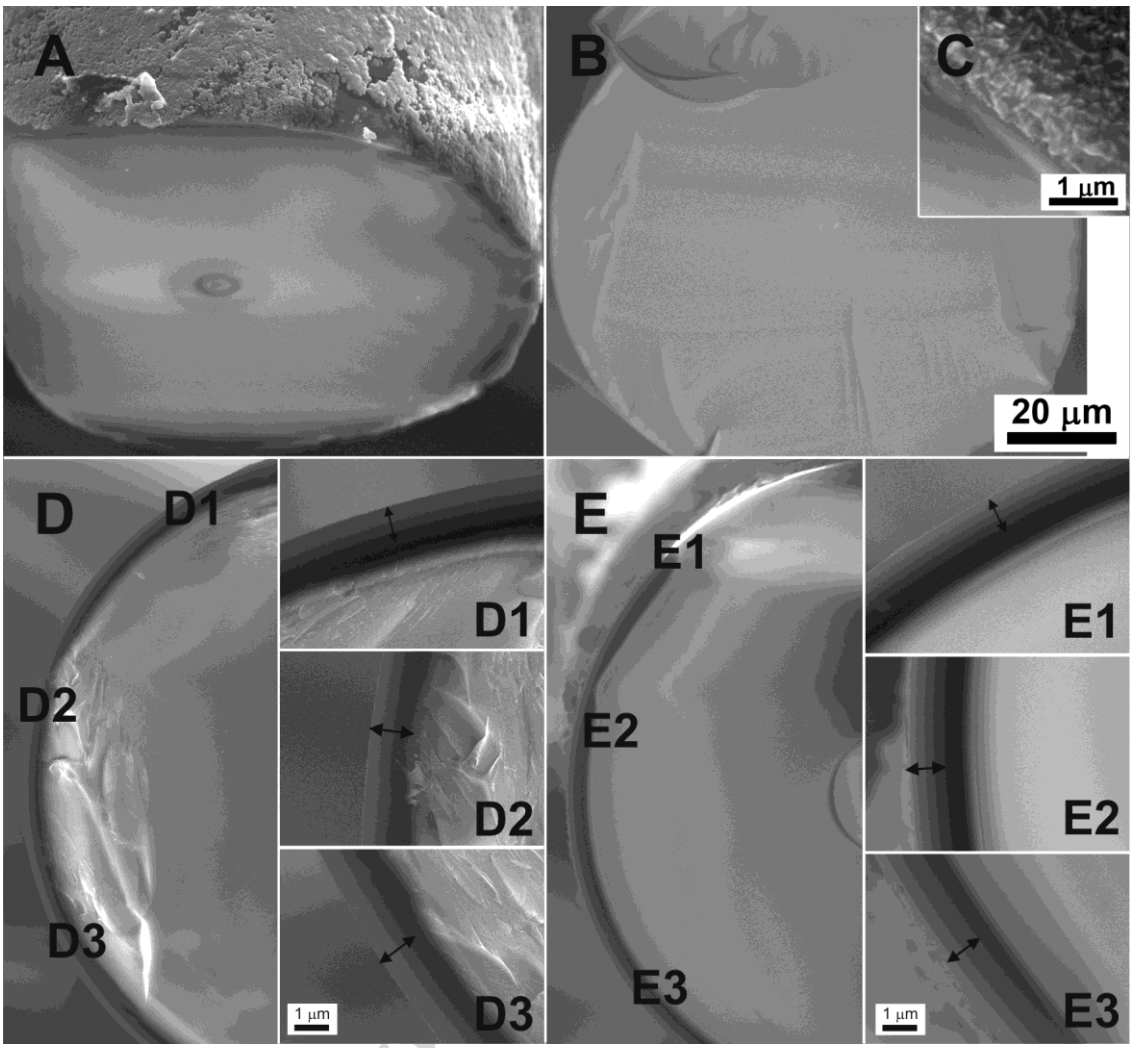

Fig. 4

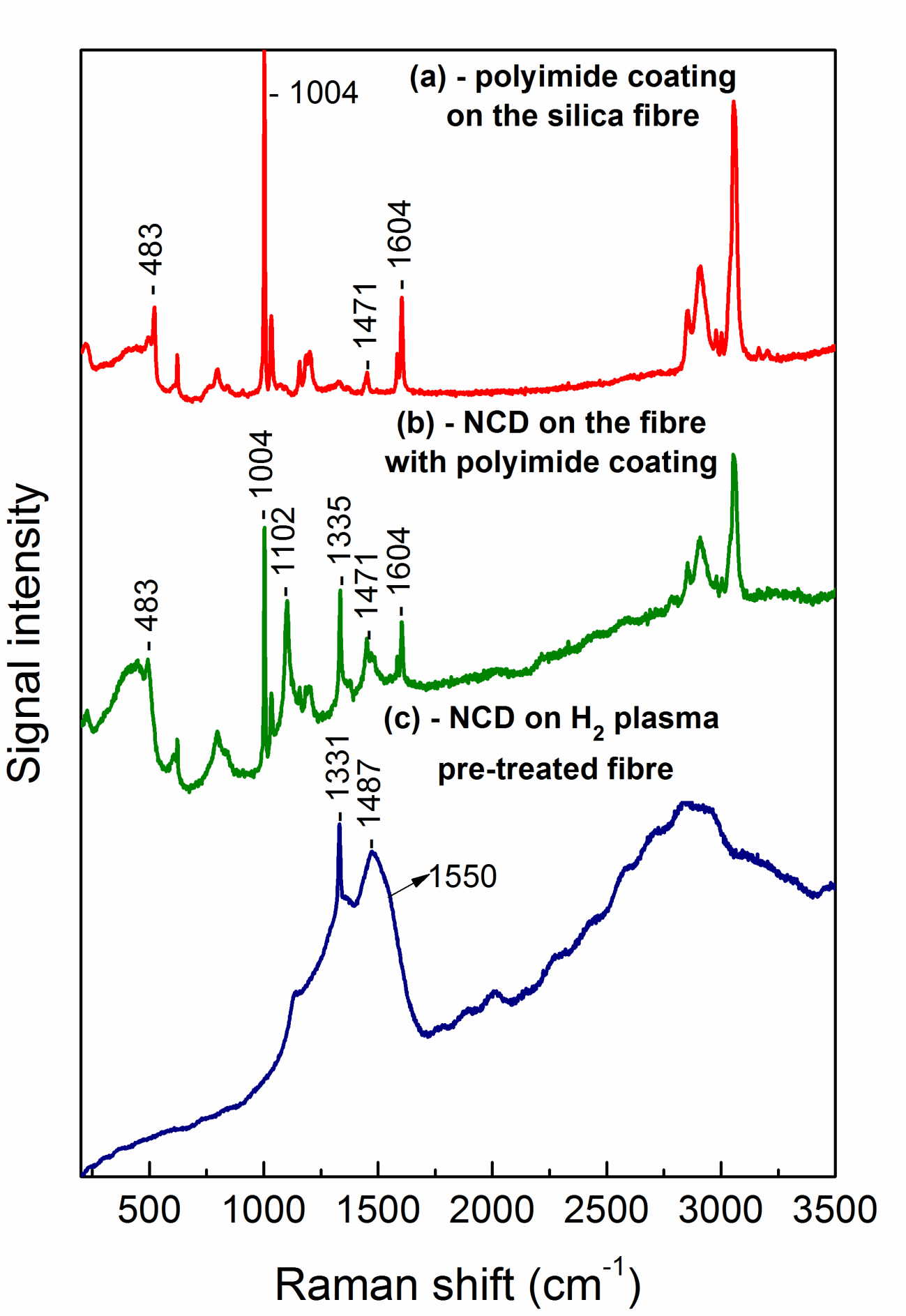
(a) - polyimide coating
on the silica fibre
- 1004
- 483
- 1471
- 1604
(b) - NCD on the fibre
with polyimide coating
- 1004
- 1102
- 1335
- 1471
- 1604
- 483
(c) - NCD on H2 plasma
pre-treated fibre
- 1331
- 1487
1550
Signal intensity
500
1000
1500
2000
2500
3000
3500
Raman shift (cm-1)

Fig. 5

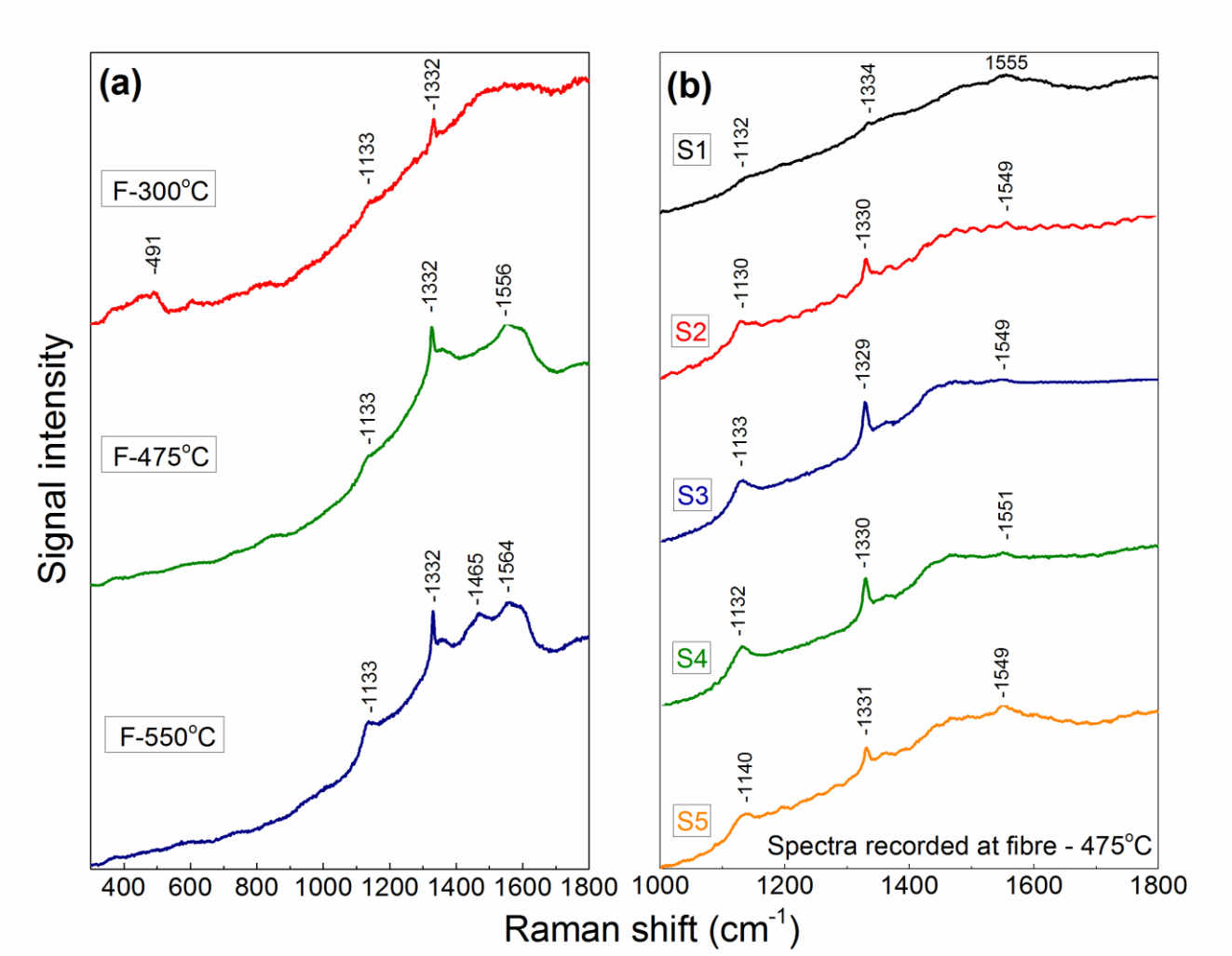

Fig. 6

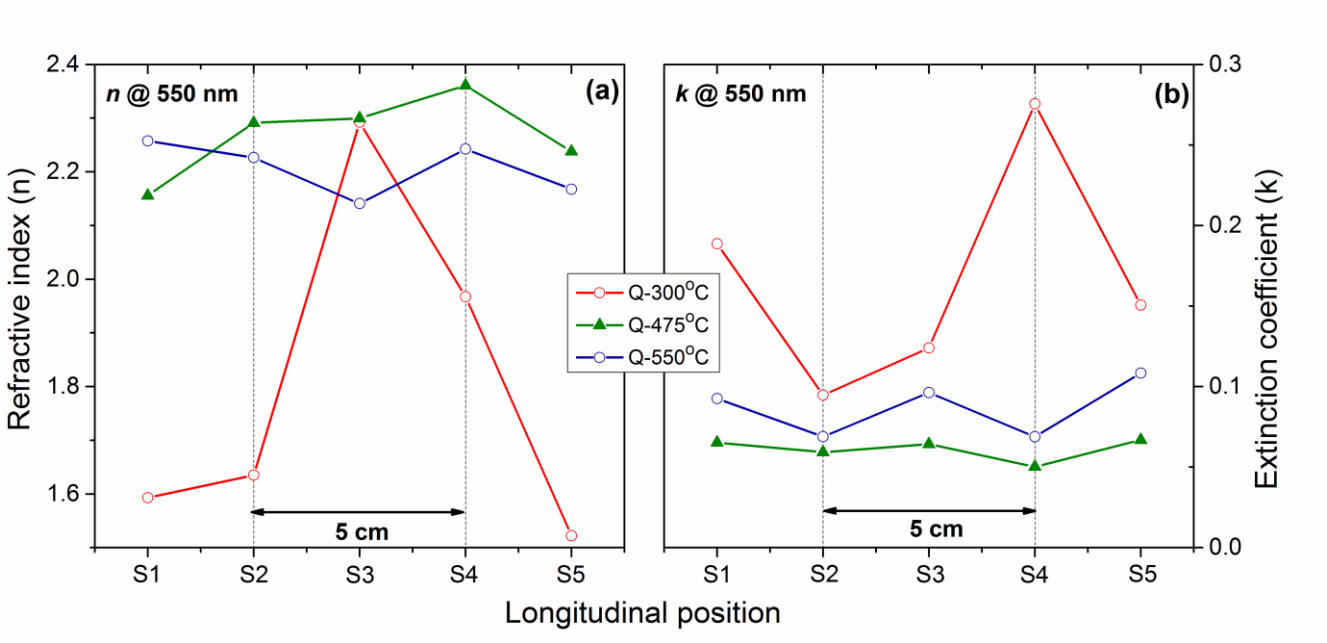

Fig. 7

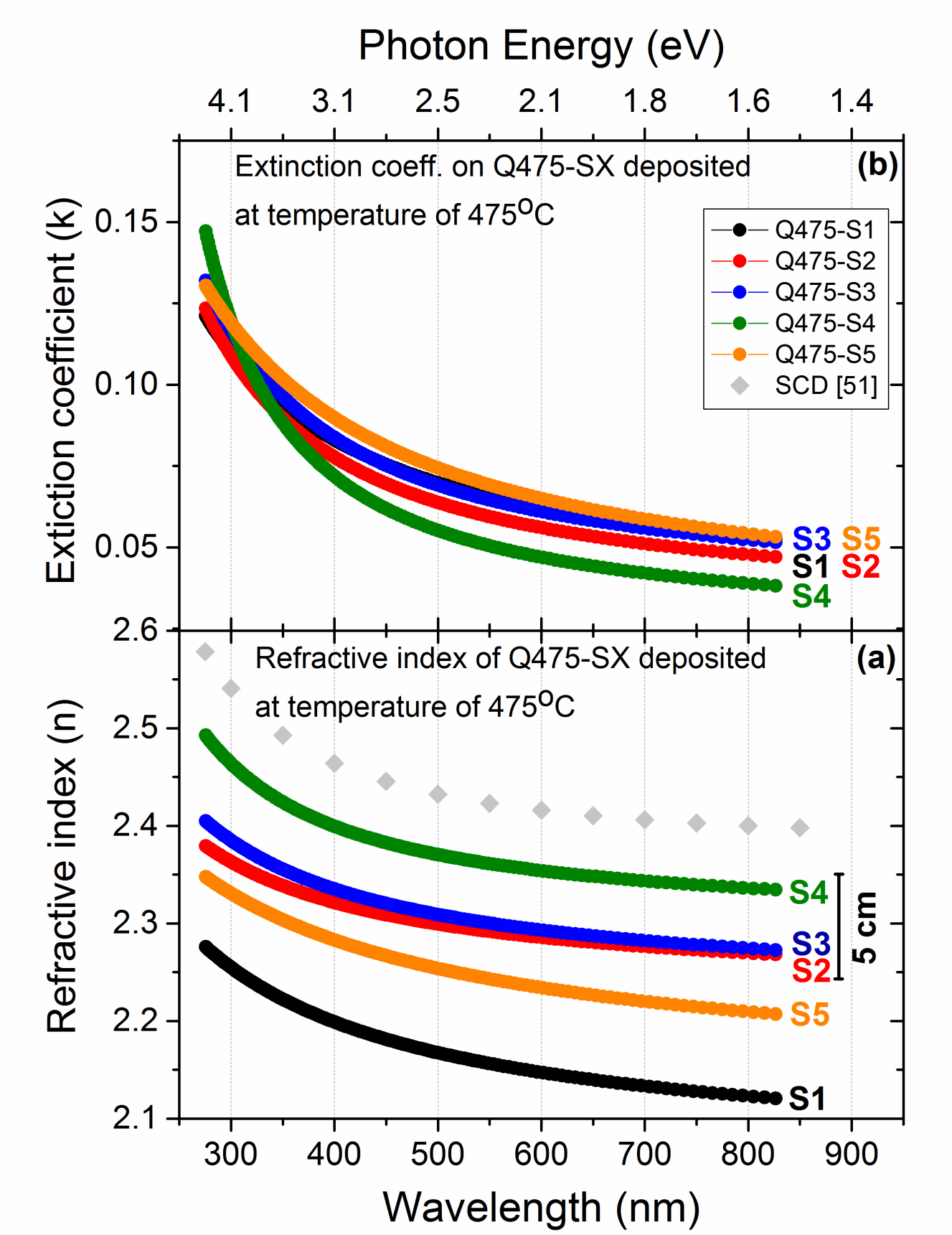

Fig. 8

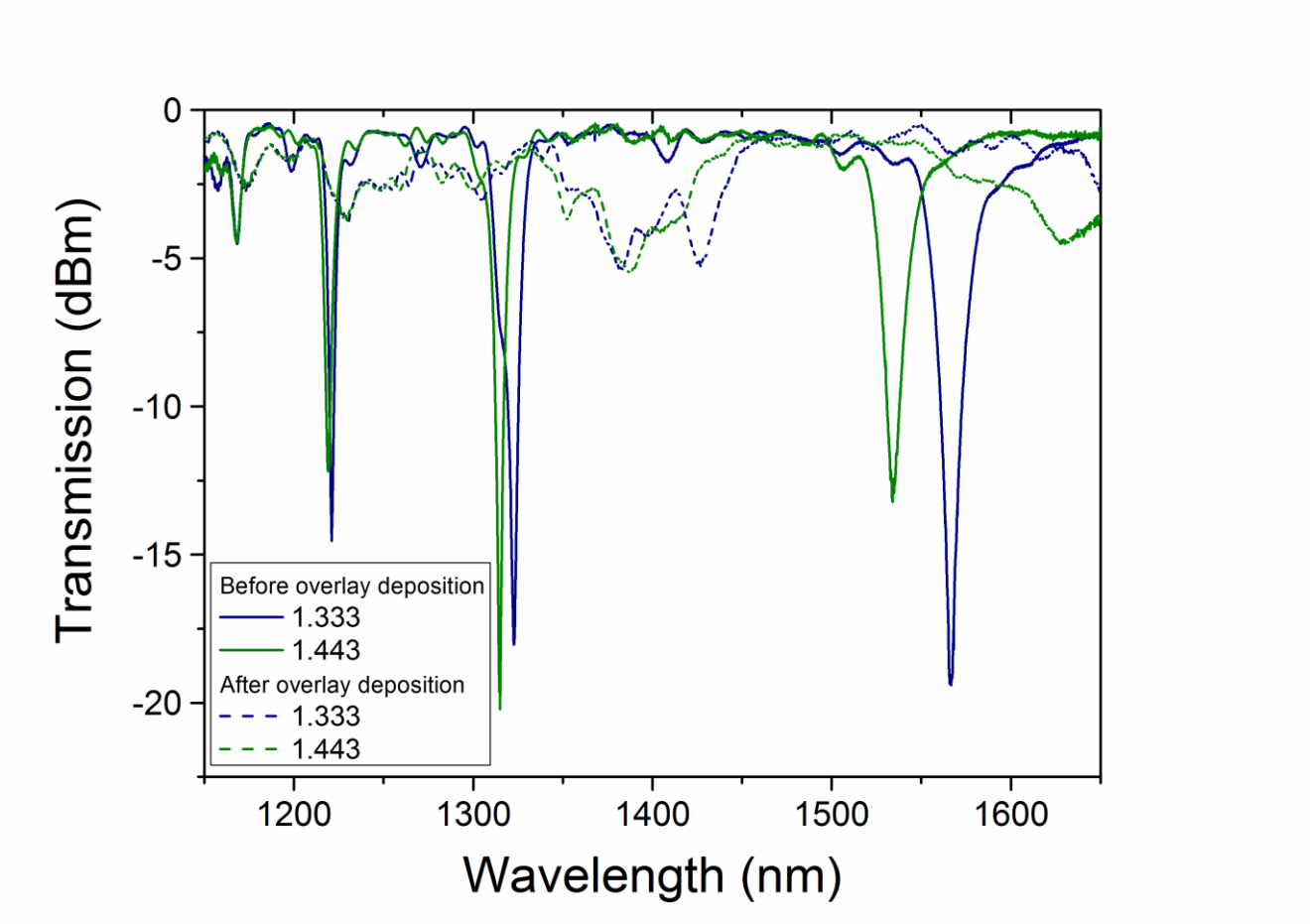

Fig. 9

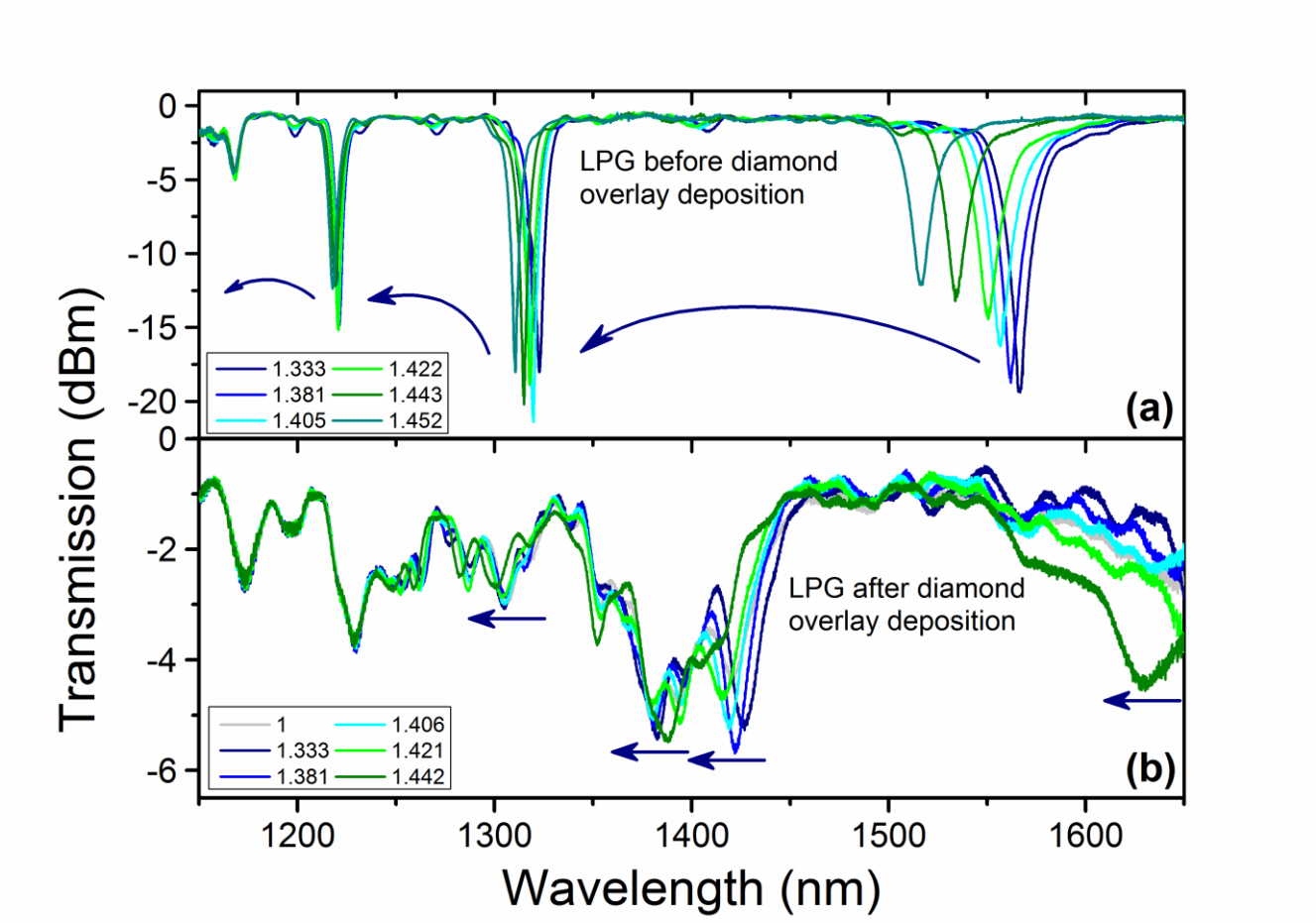

Fig. 10

Highlights:

- Growth of high refractive index NCD films on fused silica optical fibres.
- Dip-coating seeding in DND dispersed in PVA/DMSO.
- 5 cm-long homogeneous diamond film has been obtained at the fibre.
- NCD films were grown on the fibre with induced long-period grating (LPG) for sensing purposes.